Applied Catalysis B: Environmental 83 (2008) 265–276

Contents lists available at ScienceDirect

Applied Catalysis B: Environmental

journal homepage: www.elsevier.com/locate/apcatb

Al-MCM-41 catalyzed decomposition of polypropylene and hybrid genetic algorithm for kinetics analysis

B. Saha, P. Chowdhury, A.K. Ghoshal *

Department of Chemical Engineering, Indian Institute of Technology Guwahati, Guwahati 39, Assam, India

ARTICLE INFO

Article history:
Received 31 December 2006
Received in revised form 20 February 2008
Accepted 22 February 2008
Available online 29 February 2008

Keywords:
Al-MCM-41 catalyst
Hybrid genetic algorithm
Kinetics parameters
Polypropylene
Reusability

ABSTRACT

Mesoporous catalysts (Al-MCM-41) are synthesized by sol–gel and hydrothermal methods to study their effects on the catalytic decomposition of polypropylene (PP) sample. The catalysts are characterized by X-ray diffraction (XRD) analysis and nitrogen adsorption study. Since sol–gel Al-MCM-41 catalyst shows better catalytic activity, further experimental studies were conducted to find its reusability and its activity at five different heating rates. The constant pattern behaviour of the TG curves for different catalyst percentages possibly suggests existence of similar reaction mechanism where large polymer fragments are cracked on the external surface of the catalyst and then enters into the mesopores for further cracking. Thus, presence of catalyst surfaces not only converts the polymer into comparatively smaller fractions, but also makes the decomposition of PP energy effective. Kinetics parameters are estimated based on 15 different decomposition models and the multi-heating rate experimental data both for catalytic and noncatalytic decomposition of PP using hybrid genetic algorithm (HGA). Suitability of the model is tested using corrected Akaike's Information Criteria (AIC_c). Results show that Nucleation and Growth model better predicted the experimental TGA data. However, *n*th order model also shows good AIC_c score and well predicted the experimental TGA data. Thus, though apparently it seems that Nucleation and Growth model controls the decomposition of PP sample, further investigation in detail including infrared or mass spectroscopy, morphology study using SEM or TEM during such decomposition is very much essential to conclude upon the actual reaction mechanism that controls decomposition of PP sample.

1. Introduction

Catalytic pyrolysis of waste plastics has become a subject of growing interest. It not only reduces the process temperature but also produces selective and desired range of products. A large number of studies have been reported in the literatures to find the catalysts textural properties, catalytic activity, and pyrolysis product distribution. The zeolite based catalysts reduce decomposition temperature, decrease activation energy, and produce more gaseous/lighter products including the light olefins and aromatic fractions. But mesoporous catalysts accelerate the degradation process with production of low proportion of aromatics and a higher content of olefin and paraffin species. Several authors reported promising results on the catalytic pyrolysis of polypropylene over catalysts such as ZSM-5 [1–5], ZSM-12 [3], DeLaZSM-5 [4], BEA [5], MOR [5], HZSM-5 [6–9], PZSM-5 [6,9], HMOR [8], HUSY [8], US-Y [1,4,10], Beta [11], FCC [1,10], pillared clay [1], and two mesoporous catalysts SAHA [8] and MCM-41 [7,8,12]. Marcilla et al. [7] concluded that the mesoporous catalysts, with a greater pore size and higher acidity with high aluminium content (MCM-41b) was the most active for the pyrolysis of PP. According to Lin and Yen [8], MCM-41 with large mesopores and SAHA with weaker acid sites resulted in a highly olefinic product and gave a wide carbon number distribution during pyrolysis of PP.

Though MCM-41 possesses large surface area, the utilization of MCM-41 in catalysis is now restricted by its relative low acidity and low hydrothermal stability, in comparison with those of microporous zeolites. But incorporation of aluminium in the framework of MCM-41 creates Brönsted acid sites solving the problem of the low acidity that present these materials [7]. Therefore, recently a few studies using mesoporous catalyst such as Al-MCM-41 have been conducted showing excellent performance in catalytic pyrolysis of plastics. García et al. [13] showed that polyolefin cracking over ordered mesoporous Al-MCM-41 proceeds by a random scission mechanism due to its large pore size and mild acidity, yielding hydrocarbons within the gasoline and gas oil fractions. Aguado et al. [14] have reported that the

* Corresponding author. Tel.: +91 361 2582251; fax: +91 361 2582291.
E-mail address: aloke@iitg.ernet.in (A.K. Ghoshal).

0926-3373/$ – see front matter © 2008 Elsevier B.V. All rights reserved.
doi:10.1016/j.apcatb.2008.02.021

disadvantage of weaker acid properties was partly compensated by the presence of larger pores that reduced diffusional hindrances. Hydrothermal Al-MCM-41 showed the strongest acid character and exhibited the highest catalytic activity in comparison to sol–gel Al-MCM-41 and Al-SBA-15 during catalytic decomposition of LDPE and HDPE. Serrano et al. [15] have shown that Al-MCM-41 exhibited a catalytic activity comparable to *n*-HZSM-5, but significantly greater than that of larger crystal size micrometer zeolite. Further, Grieken et al. [16] reported that mesoporous aluminosilicates (Al-MCM-41, Al-MTS, Al-SBA-15) favored the oligomerization reactions, which is the important pathway for the production of higher molecular weight hydrocarbon useful as fuel.

Several pathways are known for synthesis of Al-MCM-41. They differ mainly in the use of templates, reaction temperature, time and pH of the reaction mixture and aluminium source (Table 1). However, few articles refer to the effect of MCM-41 on PP [7]. Therefore, in this present work, we have synthesized Al-MCM-41 catalyst using both hydrothermal and sol–gel methods; characterized them and reported the catalytic activities of thus synthesized Al-MCM-41 on PP using thermogravimetric analyzer (TGA) and compared the results. We have also compared the results of the present work with literature. Results showed sol–gel Al-MCM-41 to be a better catalyst for PP decomposition. Therefore, we have studied the reusability of our synthesized sol–gel Al-MCM-41 that showed promising results.

The pyrolysis kinetics study is important to know the decomposition mechanism, rate of reaction, reaction parameters and to predict the products distribution. This in turn helps in proper selection of reactor, optimization of the reactor design and operating conditions [17–19]. A few literatures have reported studies on the catalytic pyrolysis kinetics of plastics applying quantitative mechanistic kinetics model and evaluated the kinetics constants, which revealed reduction in the activation energy due to presence of catalyst [2,12]. Thermal and catalytic degradation kinetics of PP has been studied over catalysts such as silica gel, silica-magnesia, silica-titania, mordenite and silica-alumina at different heating rates using first order reaction model [20]. Further, thermal and catalytic decomposition kinetics studies of PP over BEA [5], ZSM-5 [3,5], MOR [5] and ZSM-12 [3] catalysts applying Vyazovkin model-free approach [3] and Kissinger approximation [5] based on multi-heating rates are reported in the literature. Recently, Vyazovkin model-free kinetics technique has extensively been applied for many complex reaction processes to obtain reliable and consistent kinetics information about the overall process [18,21–30]. Apart from this, the isoconversion method presents a compromise between the single-step Arrhenius kinetic treatments and the prevalent occurrence of processes whose kinetics are multi-step or non-Arrhenius [27,30]. However, information on activation energy is useless without a method of calculation of kinetics curves. For description of multistage processes the use of model-fitting methods is unavoidable and is a highway in chemical kinetics [31]. Since polymer decomposition is a complicated process, serious doubts arise about an accurate description of decomposition kinetics by using simplified equations expressing a rate of the process only via mass loss [32]. Therefore, in the absence of prior information about real kinetic mechanism, the reaction model can be chosen from a set of well-known reaction models to fit experimental data usually done in model-fitting techniques. In a number of cases, it is possible that the obtained kinetics triplet describes the rate-limiting step of the decomposition process and recommended that this approach is acceptable for chemical engineering applications [17,19,31–33]. In addition to that, a good fit of experimental results is only one condition, but it should not be the unique one. Other techniques, as for example, infrared or mass spectroscopy, morphology study

Table 1
Chemical composition and textural properties of Al-MCM-41 (present work and literature data)

Sample	BET surface area ($m^2\,g^{-1}$)	Pore volume (at $P_s/P_o = 0.9814$, adsorption) ($cm^3\,g^{-1}$)	Si/Al ratio	Al source	Si source	Template	Reference
Al-MCM-41 (sol–gel)	1202	0.7005	35.6	Aluminium isopropoxide (AIP)	Tetraethoxysilane (TEOS)	*N*-Cetyl-*N*,*N*,*N*-trimethylammonium bromide ($C_{19}H_{42}BrN$)	Present work
Al-MCM-41 (sol–gel)	1441	1.023	40	Aluminium isopropoxide (AIP)	Tetraethoxysilane (TEOS)	Hexadecyltrimethylammonium chloride ($C_{16}H_{33}(CH_3)_3NCl$)	[15]
Al-MCM-41 (sol–gel)	960	0.51	26	Aluminium isopropoxide (AIP)	Tetraethoxysilane (TEOS)	*n*-Tetradecyltrimethylammonium bromide	[50]
Al-MCM-41 (sol–gel)	978	0.70	35.6	Aluminium isopropoxide (AIP)	Tetraethoxysilane (TEOS)	Hexadecyltrimethylammonium bromide	[51]
	988	0.72	26.8	Aluminium sulfate ($Al_2(SO_4)_3{\cdot}18H_2O$	Tetraethoxysilane (TEOS)	Hexadecyltrimethylammonium bromide	
	1020	0.82	31.9	Sodium aluminate	Tetraethoxysilane (TEOS)	Hexadecyltrimethylammonium bromide	
Al-MCM-41 (sol–gel)	1270	0.83 ($P_s/P_o = 0.98$)	31	Aluminium isopropoxide (AIP)	Tetraethoxysilane (TEOS)	Hexadecyltrimethylammonium chloride ($C_{16}H_{33}(CH_3)_3NCl$)	[16]
Al-MTS(2)	1102	0.88 ($P_s/P_o = 0.6$)	30	Aluminium isopropoxide (AIP)	Tetraethoxysilane (TEOS)	Hexadecyltrimethylammonium chloride ($C_{16}H_{33}(CH_3)_3NCl$)	[53]
Al-MCM-41 (hydrothermal)	920	0.69	17.6	Sodium aluminate	Silica Ludox and tetramethylammonium silicate (TMASi)	Hexadecyltrimethylammonium chloride/ tetramethylammonium hydroxide (TMAOH)	
	811	0.73	32	Alumina	Silica Cab-O-Sil and TMASi	Hexadecyltrimethylammonium chloride/ammonia	
Al-MCM-41 (hydrothermal)	1012.3	0.804	31.9	Aluminium sulfate ($Al_2(SO_4)_3{\cdot}16H_2O$	Tetraethoxysilane (TEOS)	*N*-Cetyl-*N*,*N*,*N*-trimethylammonium bromide ($C_{19}H_{42}BrN$)	Present work
Al-MCM-41 (hydrothermal)	1100	0.84	30	$AlCl_3{\cdot}6H_2O$	Tetraethoxysilane (TEOS)	*N*-Cetyl-*N*,*N*,*N*-trimethylammonium bromide ($C_{19}H_{42}BrN$)	[16]

using SEM or TEM can be useful in order to obtain more information about processes involved [34].

In most of the reported literatures, model-fitting methods are applied to evaluate pyrolysis kinetics parameters using single heating rates and first order reaction model. However, presently, International Confederation of Thermal Analysis and Calorimetry (ICTAC) project, 2000 ruled out the validity of thermal kinetics analysis using single heating rate [35]. Modern model-fitting thermal kinetics analysis methods uses multi-heating rates; takes care of multi-step reactions and incorporates possible partial diffusion, back reaction, branch reaction, etc. in the model equations [36–39]. Still the selection of appropriate model [19,31–39], oversimplified approximation of temperature integral [25], and initial guess of kinetics parameters are major drawback of model fitting methods [37].

Recently, application of genetic algorithm (GA) or hybrid genetic algorithm (HGA) to overcome the above-mentioned problems for the estimation of kinetics parameters has attracted interest in chemical engineering, chemistry, and other fields [40–45]. GA, based on natural selection, repeatedly modifies a population of individual solutions. Over successive generations, the population "evolves" toward an optimal solution. GA is considered to have better global optimizing properties than other heuristic optimization techniques, especially, in the case of discontinuous, non-differentiable, stochastic, and highly nonlinear problems having large search spaces with many local extrema [40–47].

Therefore, in the present work, we also have reported sol–gel Al-MCM-41 catalyzed pyrolysis kinetics of PP at a catalyst percentage (18.5 wt%), after which reduction in maximum decomposition is relatively less, for five different heating rates employing the HGA technique to get the globally optimum overall kinetics parameters (activation energy, E; pre-exponential factor, k_0; and reaction order, n) using direct integration technique. In this approach, GA is used to provide initial guess for the local optimization algorithm (LOA), the direct search method used in the present work. Different physico-chemical models are used coupled with HGA to find out the best model that predicts the experimental data well. Akaike's Information Criteria (AIC) [19] is applied to choose the appropriate reaction model. Model-prediction of the experimental TGA data using the evaluated globally optimum kinetics parameters for nonisothermal catalytic and noncatalytic decomposition of PP sample is also reported.

2. Experimental

2.1. Materials

The nonisothermal decomposition with and without catalyst was carried out for polypropylene (PP) (polypropylene homopolymer (PPHP), Trade name: Koylene ADL, Grade AS030N) supplied by Indian Petrochemicals Corporation Limited, Vadodara, India with melt flow index 3.0. The sol–gel and hydrothermal Al-MCM-41 catalysts used for the present study were synthesized by the authors in the laboratory.

2.2. Synthesis of sol–gel Al-MCM-41 [50,51]

Sol–gel Al-MCM-41 was prepared according to the room temperature method described in [50,51] with template alterations. In the present case, *N*-cetyl-*N*,*N*,*N*-trimethylammonium bromide ($C_{19}H_{42}BrN$) was used as template instead of tetradecyltrimethylammonium bromide or hexadecyltrimethylammonium bromide. The catalyst was synthesized using $C_{19}H_{42}BrN$ (98%, Loba Chemie, India), tetraethoxysilane (TEOS (98%), Merck, Germany); aluminium isopropoxide (AIP (>98%), Acros Organics, India), 25% ammonia solution ((99.5%), Merck, India), propan-2-ol (PrOH) ((99.5%), Merck, India) and deionized water. The low concentration (3.7%) solution of AIP in PrOH was prepared in a glass tube by mixing in an ultrasonic bath for 10–15 min. The template (1.29 g) was mixed with 69.2 g of water, warmed up until complete dissolution, and allowed to cool down before adding 5 mL of ammonia. To this, a mixture of 5 mL of TEOS with an appropriate volume of the AIP solution was added dropwise, while stirring, over a period of 15 min to achieve the required molar ratio. The molar composition of the gel was 1TEOS:1/xAIP:0.147C19TMABr:3.04NH_3:160H_2O:yPrOH, with $y = 2.89$ and $x = 30$. The suspensions were kept under stirring for 1–1.2 h.

2.3. Synthesis of hydrothermal Al-MCM-41 [52]

Hydrothermal Al-MCM-41 was synthesized according to the procedure described in [52]. NaOH (0.40 g) and $C_{19}H_{42}BrN$ (0.6 g) were dissolved in 32 mL deionized water. TEOS (3.85 g) was added to the mixture. Aluminium sulfate ($Al_2(SO_4)_3{\cdot}16H_2O$, Merck, India) (0.37 g) was dissolved in 10 mL of deionized water in a separate beaker and was then added to the reaction mixture. Stirring was continued for about 105 min at ambient temperature. The resulting mixture was stirred and heated at 80 °C for 20 min. The mixture was further stirred overnight and then was transferred to a Teflon-lined autoclave at 150 °C for 12 h. The molar composition of the gel was 1.0SiO_2:0.031Al_2O_3:0.27Na_2O:0.089CTA^+:130H_2O [52].

In both sol–gel and hydrothermal methods, the synthesized products were recovered by filtration and washed with about 2 L of deionized water. After drying at 343 K, the samples were calcined in air at 823 K for 12 h. A heating rate of 2 K min^{-1} was maintained during the course of time.

2.4. Characterization of Al-MCM-41 catalysts

Al-MCM-41 catalysts were characterized by X-ray diffraction (XRD) analysis and nitrogen adsorption study at 77 K. The XRD was carried out on Bruker AXS D8 Advance instrument equipped with the graphite monochromatized Cu Kα radiation, $\lambda = 1.5406$ Å (40 kV, 40 mA) in 2θ angles ranging from 5° to 85° with a step size of 0.05 and step time of 0.5 s. The surface area, pore volume and pore size distribution were measured in BET surface area analyzer (Beckman-Coulter SA 3100) using Nitrogen adsorption isotherm at 77 K. The relative pressure used to obtain the BET area is in the range 0.05–0.2. The value of the C (constant of BET equation) is 71.28 for hydrothermal process and 34.025 in sol–gel method. All Al-MCM-41 samples were thoroughly outgassed for 3 h at 300 °C to remove any moisture or volatile materials adhering to it. Particle size analysis of the catalyst particles was carried out in a laser particle size analyzer (MASTERSIZER 2000) and the average particle size is found to lie within 20–30 μm.

2.5. Catalytic decomposition of PP over Al-MCM-41 catalysts (sol–gel and hydrothermal)

Thermal and catalytic decomposition experiments were carried out in a TGA instrument of Mettler TOLEDO with model no. TGA/SDTA 851^e under nitrogen atmosphere for a range of temperature 303–873 K. Nitrogen flow rate was maintained at 40–50 mL min^{-1} according to the specification of the equipment. PP samples were shredded into very small pieces of −40/+60 mesh size and directly fed to the TGA instrument. Platinum crucible (150 μL) was used as sample holder. PP decomposition experiments were carried out with different percentage of catalysts (0–33 wt%) at 10 K min^{-1} (Table 2). Our preliminary analysis showed that sol–gel Al-MCM-41 was better performing

Table 2
Experimental conditions for TGA studies using different catalysts

Catalysts	Catalysts percentage (%)	Total initial mass (mg)	T_m (K)
Al-MCM-41 (sol–gel)	7.7	9.53	652.53
	13.1	12.19	636.89
	16.4	19.09	625.81
	18.5	10.81	619.6
	21.6	10.7	616.69
	24.6	10.54	611.63
	32.5	12.11	608.98
Al-MCM-41 (hydrothermal)	5.1	9.69	677.4
	10.9	9.85	674.4
	17.1	10.44	658.8
	20.8	9.81	666.8
	25.5	10.28	654.7
	33.2	9.92	655.1

than hydrothermal Al-MCM-41 in terms of reduction in maximum decomposition temperature. The optimum catalyst percentage was found around 18.5 wt% for sol–gel catalyst after which reduction in maximum decomposition temperature with increase in catalyst percentage was not so significant. Therefore, further catalytic decomposition experiments were carried out using 18.5 wt% catalysts (sol–gel Al-MCM-41) at different heating rates of 5, 10, 15, 20, and 25 K min^{-1}. The experimental conditions are summarized in Table 3. The TGA experiments were repeated thrice at 10 K min^{-1} heating rate without catalysts. The deviations observed are very little. However, the deviations are reported in terms of average relative deviation, ARD $(\%) = (100/N)\sum_{i=1}^{N} |(x_i^{exp} - x_{av,i})/x_{av,i}|$, where x_i^{exp} and $x_{av,i}$ are the experimental values of the variables (temperature and normalized mass) and average values of the variables, respectively, and i = no. of data points for each experiment. Results show that ARD(%) are 0.005–0.019 (for temperature), 0.041–0.1579 (for mass). Thermal decomposition (noncatalytic) experiments for PP were also conducted in dynamic condition at different heating rates of 5, 10, 15, 20 and 25 K min^{-1}. It may be noted that the marginal differences that may arise due to the different heat flow resistances due to the differences in the sample amount between the catalytic and noncatalytic cases are neglected.

2.6. Reusability of Al-MCM-41 (sol–gel)

Since sol–gel Al-MCM-41 was better performing than hydrothermal Al-MCM-41 in terms of reduction in maximum decomposition temperature, reusability study of the catalysts was performed by reusing the catalyst at 17 wt% for seven consecutive runs at 10 K min^{-1} maintaining identical experimental conditions. The experimental conditions are summarized in Table 4.

Table 4
Experimental conditions for reusability test

Run no.	Mass of PP (mg)	Mass of Al-MCM-41 (sol–gel) (mg)	% Cat	T_m (K)
1	15.84		17.0	625.81
2	16.29		16.6	627.39
3	15.95	3.25	16.9	631.46
4	15.89		17	633.69
5	15.87		17	643.78
6	16.19		16.7	643.93
7	15.97		16.9	649.93

3. Kinetics analysis

3.1. Multi-heating rates model-fitting method for nonisothermal experiments [19,31–39]

The nth order kinetic model equation combined with the Arrhenius approach of the temperature function of reaction rate constant is:

$$\frac{d\alpha}{dt} = k_0 \exp\left(-\frac{E}{RT}\right) f(\alpha) \quad (1)$$

where t is the time (min), T the temperature (K), α the conversion of the reaction ($\alpha = (W_0 - W)/(W_0 - W_\infty)$), where W_0 is the initial weight of the sample, W_∞ the final weight of the sample and W that at any temperature T (all weights given in mg), $d\alpha/dt$ is the rate of the reaction (min^{-1}) and $f(\alpha)$ the reaction model, k_0 is the pre-exponential factor (K^{-1}) and E the activation energy (kJ/mol) are the Arrhenius parameters, R is the universal gas constant (kJ/mol K). The reaction model may take various forms based on nucleation and nucleus growth, phase boundary reaction, diffusion, and chemical reaction. In the present investigation, we have applied different such models (Table 5) for catalytic decomposition kinetics using single step and multi-heating rates. The optimization approach is that of multi-parameter optimization.

At a constant heating rate for nth order reaction model under nonisothermal conditions the explicit temporal/time dependence in Eq. (1) is eliminated through the trivial transformation

$$\beta\frac{d\alpha}{dT} = k_0 \exp\left(-\frac{E}{RT}\right)(1-\alpha)^n \quad (2)$$

where $\beta = dT/dt$ is the heating rate (K min^{-1}) and $d\alpha/dT$ is the rate of reaction (K^{-1}). Eq. (1) can be integrated as:

$$g(\alpha) = \int_0^\alpha \frac{d\alpha}{f(\alpha)} = \frac{k_0}{\beta}\int_0^{T_\alpha} \exp\left(-\frac{E}{RT}\right) dT = \frac{k_0}{\beta} I(E,T) \quad (3)$$

Table 3
Experimental conditions for catalytic (Al-MCM-41 (sol–gel)) and noncatalytic TGA studies

Sample	Initial mass (mg)	Heating rate (K min^{-1})	Temperature range (K)	$T_{w0}/T_d/T_m/T_{w\infty}$ (K)
PP	19.77	5	303–875	533.6/596.9/706.8/773.9
	20.32	10	303–875	526.9/670.0/723.07/749.8
	20.67	15	303–875	527.8/684.6/731.4/777.6
	19.78	20	303–875	527.5/684.8/736.8/770.2
	19.41	25	303–875	527.1/696.6/742.9/785.7
PP + Al-MCM-41 (18.5 wt%)	7.48	5	303–873	489.3/535.1/608.6/669.9
	10.35	10	303–873	473.2/576.6/619.6/682.3
	13.59	15	303–873	461.7/596.3/637.6/700.9
	10.80	20	303–873	464.4/605.2/640.7/717.5
	9.09	25	303–873	461.9/607.9/649.0/711.0

Table 5
The equation for calculation of kinetics parameters and AIC_c results [31,32]

Kinetic models	Kinetic functions, integral of kinetics function and calculation of α where $x = (k_{0i}/\beta_l)I(E_i, T_{i,l})$	Order	Model no.	AIC_c score	
				PP samples	PP + Al-MCM-41 samples
Nucleation and Growth	$f(\alpha) = (1/n)(1-\alpha)(-\ln(1-\alpha))^{1-n}$ $g(\alpha) = [-\ln(1-\alpha)]^n$ $\alpha = 1 - \exp(-x^{1/n})$	$n = 1/4$	1	1006.2	−573.672
		$n = 1/3$	2	542.29	2232.016
		$n = 1/2$	3	−433.58	−2081.74
		$n = 2/3$	4	−1150.03	−2697.39
Chemical reaction	$f(\alpha) = (1-\alpha)$ $g(\alpha) = -\ln(1-\alpha)$ $\alpha = 1 - \exp(-x)$	$n = 1$, 1st order	13	−675.54	−2056.68
		$n = 2$, 2nd order	14	381.7632	−1181.07
		$n = n$, nth order	15	−830.97	−2054
	$f(\alpha) = (1-\alpha)^n$ $g(\alpha) = [1/(1-\alpha)^{n-1} - 1]/(n-1)$ $\alpha = 1 - [1 + (n-1)x]^{1/(1-n)}$				

Now, for nonisothermal condition and jth data point, integral form of Eq. (3) can be written as:

$$g(\alpha_j) = \int_0^{\alpha} \frac{d\alpha}{f(\alpha_j)} = \frac{k_0}{\beta}\int_0^{T_{\alpha_j}} \exp\left(-\frac{E}{RT_{\alpha_j}}\right) dT = \frac{k_0}{\beta} I(E, T_{\alpha_j}) = x \quad (4)$$

The temperature integral (Eq. (4)) can be evaluated by several popular approximations and direct numerical integration as reported in our recent publications [18,19,29,30]. We used the technique of direct numerical integration [29,30] for the same, where the temperature integral takes the form

$$I(E,T) = \int_0^T \exp\left(-\frac{E}{RT}\right) dT = \frac{E}{R}\left[\frac{\exp(-u)}{(u)} - E(u)\right] \quad (5)$$

where $u = E/RT$ and $E_i(u) = \int_u^{\infty} \exp(-u)/u\, du$.

This equation can be solved for α_j using different reactions models reported in Table 5.

For example, the nth order kinetic model equation is solved by substituting $(k_0/\beta) = \exp(\tilde{K}_0)$ where $K_0 - \ln(\beta) = \tilde{K}_0$ and $k_0 = \exp(K_0)$ and transforming Eq. (4) for nth order chemical reaction model as follows:

For $n \neq 1$,

$$\alpha = 1 - [(\exp(\tilde{K}_0))I(E,T)(n+1) + 1]^{1/(n+1)} \quad (6)$$

For $n = 1$,

$$\alpha = 1 - \exp[-(\exp(\tilde{K}_0))I(E,T)] \quad (7)$$

3.2. Multi-parameter optimization

The objective function most frequently used in case of multiple heating rates to calculate optimum values of $\Delta(E, K_0, f_m(\alpha_l))$ for mth model, total L heating rates and total J data points by minimization of square of deviation between experimental mass ($M_{Exp}(T)$) and calculated mass ($M_{Cal}(T)$) is given by the following equation:

$$\Delta(E, K_0, f_m(\alpha_l)) = \sum_{l=1}^{L}\left[\sum_{j=1}^{J}[M_{Exp,l,j} - M_{Cal,l,j}]\right]^2 \quad (8)$$

The values of $M_{Cal,i,l,j}$ calculated for each single value of $\alpha_{Cal,i,l,j}$ are as follows:

$$M_{Cal,l,j} = M_{Exp,l,0} - \alpha_{l,j}(M_{Exp,l,0} - M_{Exp,l,\infty}) \quad (9)$$

where $M_{Exp,l,0}$ is the initial point and $M_{Exp,l,\infty}$ is the final point lth heating rate. However, in the present work all models except nth order reaction model involved two parameters optimization since in those models E, K_0 values are optimized for different models of $f_m(\alpha_l)$ in Table 5.

3.3. Akaike's Information Criteria (AIC)

Akaike's Information Criteria (AIC), discussed below is applied to choose the appropriate reaction model.

$$AIC = N\ln\left(\frac{SS}{N}\right) + 2K \quad (10)$$

where N is the number of data points, K is the number of parameters plus one and SS is the sum of square of vertical distance of the points from the centre. The corrected AIC for small number of data points is obtained from the following equation:

$$AIC_c = AIC + \frac{2K(K+1)}{N-K-1} \quad (11)$$

Thus for two reaction models A and B,

$$\Delta AIC = AIC_{C,B} - AIC_{C,A} \quad (12)$$

$AIC_{C,B}$ is corrected AIC for model B and $AIC_{C,A}$ is corrected AIC for model A.

3.4. The structure of a hybrid genetic algorithm [40,45–49]

GA employs a probabilistic approach and has better global optimizing properties but shows poor convergence to optimality. Whereas, HGA uses a typical basic GA with elitist strategy to reach near gradient or/direct-based search method shows faster convergence to global optima. Therefore, often GA is hybridized using a LOA to improve its performance as a global optimization technique while overcoming the limitations of poor convergence and weak exploitation capabilities. The various kinds of hybridizations using LOA are pre-hybridization, organic-hybridization and post-hybridization [48].

3.5. Structure of HGA used for the present work [49]

In the present work, we have used post-hybridization method, i.e. GA coupled with LOA, where GA is used to provide an initial design for LOA. This kind of hybridization seems to be the best way of combining the best characteristics of the two approaches as no compromise is made on the global and local optimizing characteristics [48]. We have used the default initial population size (20), the default creation function 'Uniform' to create a random initial population with a uniform distribution, the stochastic options from the GA toolbox that chooses parents for the next generation, Gaussian function for mutation, scattered function for the next generation, forward migration option for the movement of individuals between subpopulations, default value of migration fraction (0.2) for migration of individuals between subpopulation, value of interval as 20, i.e. migration between subpopulations takes place every 20 generations, multidimen-

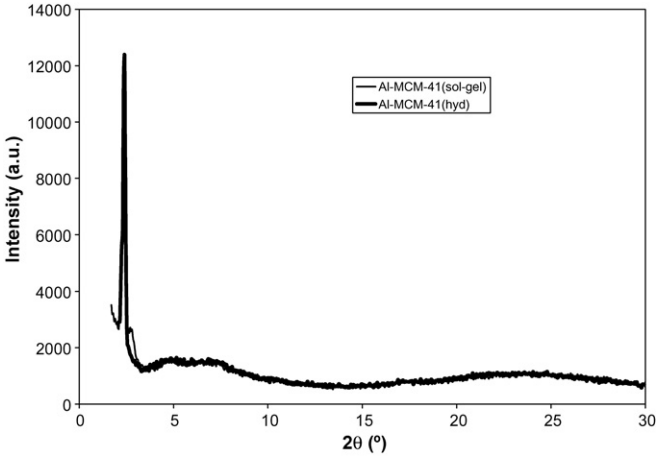

Fig. 1. XRD pattern of Al-MCM-41 (sol–gel and hydrothermal) catalyst (using step size = 0.05° and step time 0.5 s).

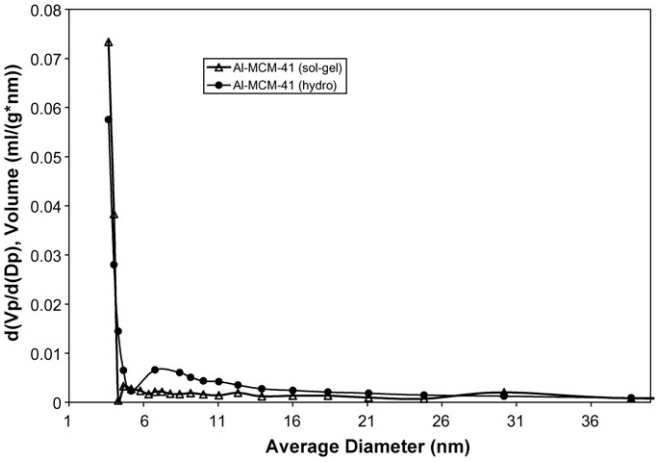

Fig. 3. BJH (adsorption) pore size distribution of Al-MCM-41 (sol–gel and hydrothermal) catalysts.

sional unconstrained nonlinear minimization function 'fminsearch' as the hybrid function that uses the final point from the genetic algorithm as its initial point, and specified only the number of generation as stopping criteria.

The optimized kinetics triplet obtained by the above configured HGA showed pretty good prediction of the experimental TGA decomposition data. However, further improvement on the HGA configuration can be made through optimization of configuration through several runs, which is not concentrated upon in the present work.

4. Results and discussion

4.1. Characterization of Al-MCM-41 catalyst

The powder XRD patterns (Fig. 1) of the synthesized Al-MCM-41 catalyst (after calcination) from both sol–gel and hydrothermal routes exhibit the low angle and intense diffraction peak between $2\theta = 2.1–2.40^\circ$ indicating the reflection of [1 0 0] plane [16]. No peak at higher angle was observed indicating the absence of any crystalline phase containing aluminium [51].

Nitrogen adsorption isotherms at 77 K for both sol–gel and hydrothermally synthesized Al-MCM-41 catalysts are shown in Fig. 2. Both the catalysts show similar trends which is a type IV isotherm according to IUPAC classification, typical of good quality mesoporous materials [16,51]. In case of hydrothermal route, the isotherm is completely reversible but the sol–gel route shows a clear hysteresis which is understandable as at higher relative pressure (P_s/P_o) there is pore filling, indicating size uniformity of the tubular unidirectional mesopores [51]. Table 1 summarizes the textural properties of Al-MCM-41 catalysts prepared by sol–gel and hydrothermal methods. Al-MCM-41 (sol–gel) samples have higher Si/Al ratio and higher BET surface area than Al-MCM-41 (hydrothermal). The pore size distributions were calculated using the Barrett–Joyner–Halenda (BJH) model applied to the adsorption branch of the isotherm, assuming cylindrical pore geometry. It was found that the pore sizes lie within 4 nm in both the cases (Fig. 3). The total distribution (beyond 3 nm) could not be possible due to instrumental limitation. However, Fig. 3 and Table 1 indicate that both the samples have pore size uniformity and considerable high pore volumes and surface areas, characteristic of mesoporous materials. Pore volumes were determined from the nitrogen adsorbed volume at $P/P^0 = 0.98$.

4.2. Catalytic activity of sol–gel and hydrothermal AL-MCM-41 for PP decomposition

Experiments were conducted for both catalytic and noncatalytic dynamic decomposition of PP in TGA. The temperature at which maximum weight loss rate occurs (T_m) is reported in Table 2

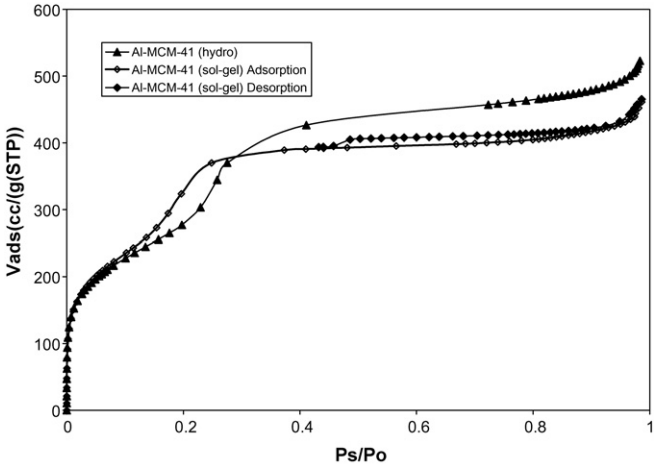

Fig. 2. Nitrogen adsorption isotherm at 77 K of Al-MCM-41 catalysts.

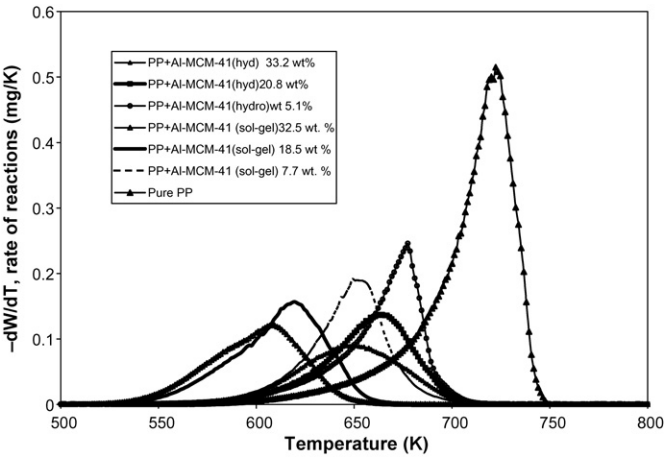

Fig. 4. Experimental DTG curves for the catalytic pyrolysis of waste PP with different catalyst (Al-MCM-41 (sol–gel and hydrothermal)) percentage.

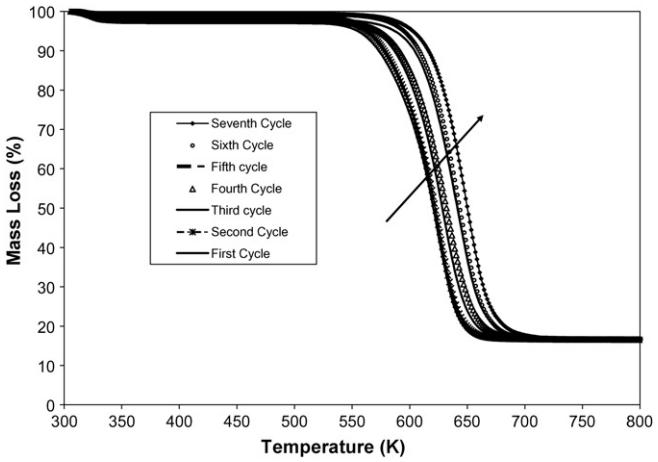

Fig. 5. Experimental TG curves for the different cycles of catalytic pyrolysis of PP with 17% catalyst (Al-MCM-41 (sol–gel)).

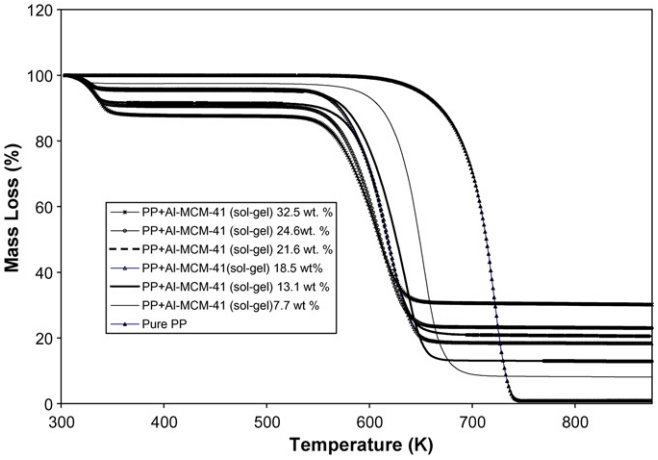

Fig. 7. Experimental TG curves for the catalytic pyrolysis of waste PP with different catalyst (Al-MCM-41 (sol–gel)) percentage.

for each case of the experiments. Reduction in T_m on application of catalysts (sol–gel and hydrothermal Al-MCM-41) is shown through the sample derivative thermogravimetric (DTG) curves (Fig. 4). It is observed from both the table and the figure that T_m reduces significantly, in comparison to noncatalytic decomposition, due to application of the catalyst. It is further observed that the sol–gel Al-MCM-41 is much more effective than the hydrothermal one in reducing the T_m for PP. Table 3 reflects that thermal decomposition temperatures of PP are shifted to much lower temperatures in the presence of catalysts. The maximum shifts of T_m are observed to be 114 K and 68 K for sol–gel (32.5 wt%) and hydrothermal (25.5 wt%) catalysts, respectively. According to Aguado et al. [14], hydrothermal Al-MCM-41 was more effective than sol–gel one towards decomposition of LDPE and HDPE. The reduction in maximum decomposition temperatures for LDPE and HDPE using hydrothermal Al-MCM-41 were reported to be 69 and 58 K, respectively. Again, Marcilla et al. [7] reported that Al-MCM-41 should show better catalytic activity towards PP than LDPE. Thus, our present result conforms to the observations of Marcilla et al. [7]. It is worth mentioning that catalytic activity of mesoporous catalysts like MCM-41 towards polymer decomposition mainly depends on the mesopore size that allows the movement of the polymer chain in the pores, surface area that takes part in the decomposition reaction and the aluminium content (or number of acid sites), which is involved in such decomposition mechanism [7]. Table 1 and Fig. 3 imply that the catalysts synthesized in the present study have almost the similar pore size and similar Si/Al ratio but they have widely different surface areas, which possibly makes the differences in the catalytic activities.

4.3. Reusability study of sol–gel Al-MCM-41 catalyst

Since we found sol–gel Al-MCM-41 catalyst to perform better over hydrothermal Al-MCM-41, we studied the reusability of the sol–gel Al-MCM-41 catalyst. For that purpose, we had taken 17 wt% catalyst mixed with the PP sample and studied the decomposition behaviour in TGA. The same catalyst was repeatedly used for seven times to see the effect on decomposition behaviour. Fig. 5 represents the thermogravimetric (TG) plot for the repeatedly used sol–gel Al-MCM-41 (17 wt%) catalyzed decomposition of PP. It can be observed from Table 4 that the catalyst activity is reduced slowly (also evident from Fig. 5), where T_m is increased from 353 °C (first cycle) to 377 °C (seventh cycle). This indicates that the catalyst is able to maintain its activity fairly well even after the seventh cycle which is also evident from the XRD plot of the catalyst after the seventh cycle (Fig. 6). Thus, the present sol–gel catalyst is a promising one for industrial applications.

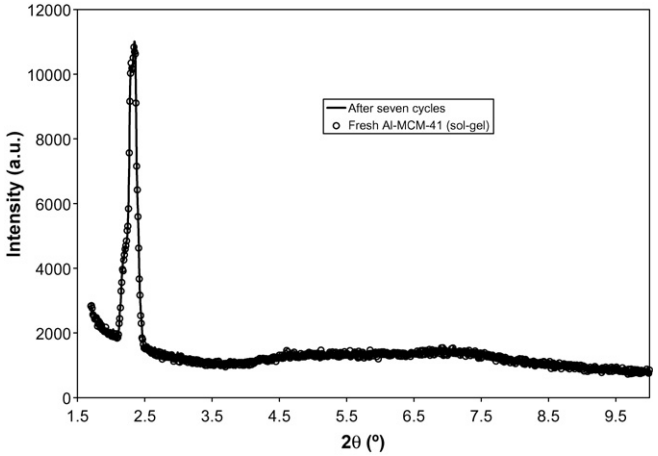

Fig. 6. XRD pattern of Al-MCM-41 (sol–gel) catalyst after seventh cycle (using step size = 0.05° and step time 0.5 s).

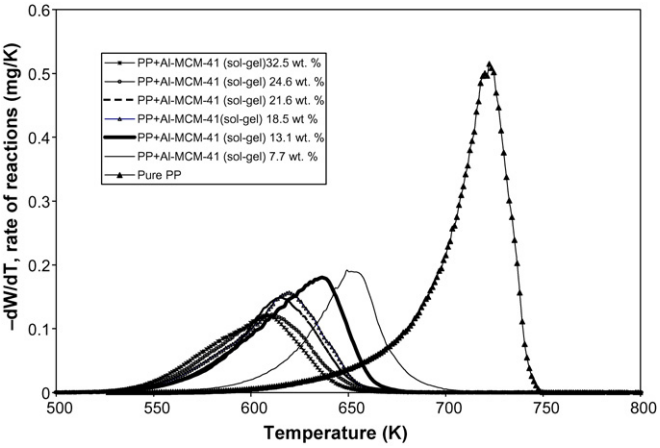

Fig. 8. Experimental DTG curves for the catalytic pyrolysis of waste PP with different catalyst (Al-MCM-41 (sol–gel)) percentage.

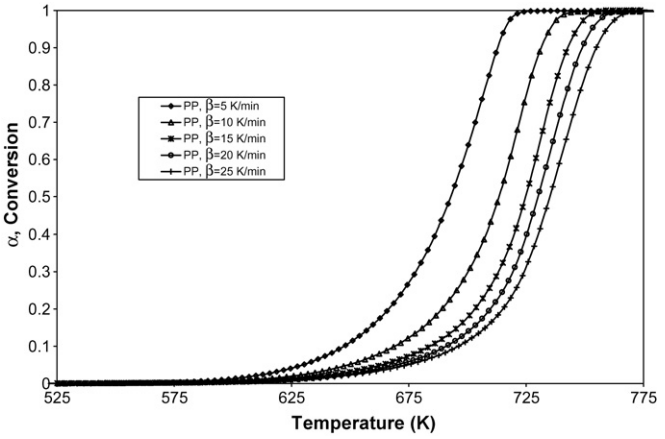

Fig. 9. Variation of conversion (α) with temperature during nonisothermal pyrolysis of PP sample at multiple heating rates.

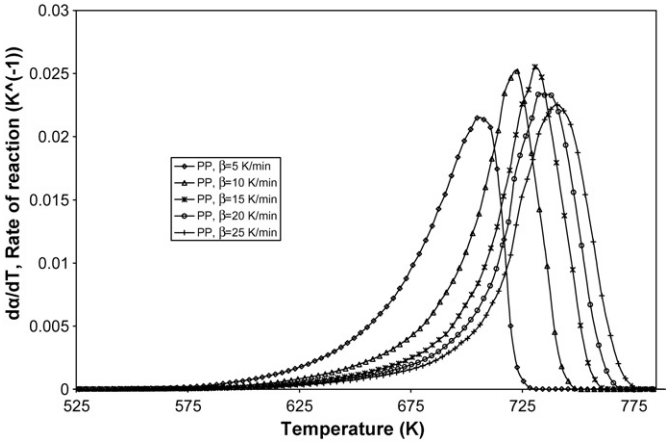

Fig. 10. Variation of rate of decomposition ($d\alpha/dT$) with average temperature during nonisothermal pyrolysis of PP sample at multiple heating rates.

4.4. Determination of optimum catalyst (sol–gel Al-MCM-41) concentration

Figs. 7 and 8 illustrate the thermogravimetric (TG) and the derivative thermogravimetric (DTG) plots, respectively for the sol–gel Al-MCM-41 catalyzed decomposition of PP. It can be observed from Fig. 7 that the weight loss observed at low temperature is due to loss of present moisture in the catalyst. The percentage weight loss is found to be increased with an increase in catalyst percentage. It is further observed from the figures that the shape of the curves changes significantly up to 15 wt% of the catalyst. From catalyst composition of 15 wt% onwards, the curves are overlapping in nature indicating less impact of the catalyst. Since the catalysts are expensive and, at the moment, there are no useful ways to improve their short life or to make effective recycling [12], therefore, we concentrated on getting the optimum catalysts percentage. Fig. 9 shows the gradually decreasing effect of catalyst percentage on the change in T_m with respect to that for noncatalytic PP decomposition, ΔT_m. It is further observed that the optimum catalyst percentage could be around 18.5 wt%, since, after that reduction in T_m with increase in catalyst percentage is not so significant. The reduction in maximum decomposition temperature is around 103 °C at 18.5 wt% catalyst. Thus, we selected 18.5 wt% as the optimum catalyst (sol–gel Al-MCM-41) percentage for the present study. It is also interesting to see from Fig. 7 that TG curves with and without catalysts are constant pattern in nature. Only shifts in the TG curves towards lower temperatures are observed due to application of catalyst and increase in catalyst percentage. This shift of the curves also slowly reduced at higher percentages of the catalyst indicating less effect of addition of further catalyst in the polymer sample. However, this behaviour is contrary to our recent reports on the catalytic activity of ZSM-5 on LDPE [30], where catalytic decomposition continued for a wider range of temperature than noncatalytic decomposition leading to flatter TG curves. This behaviour [30] suggested the possible existence of a different reaction mechanism due to the microporous zeolite catalyst compared to noncatalytic decomposition of LDPE. Here, large polymer fragments are cracked on the external surface of the catalyst at the start of degradation forming smaller molecules and radicals via end-chain cracking pathway. These molecules in the subsequent stages enter into the pores and participate in other reactions like isomerization and oligomerization. Therefore, catalytic (ZSM-5) degradation of LDPE results in formation of aromatics, light paraffin and olefins due to the reactions like oligomerization, cyclization, and hydrogen transfer reactions. The aromatics yield increased where subsequent steps of cyclization occurred at higher temperatures [30]. But, in the present work the constant pattern behaviour of the TG curves possibly suggests existence of similar reaction mechanism both under catalytic and noncatalytic decomposition of mesoporous Al-MCM-41. Here, large polymer fragments are cracked on the external surface of the catalyst and then enter into the mesopores where they get cracked further leading mainly to the higher olefins and liquid products [8,15]. This can only be confirmed after thorough analysis of the decomposition products. However, the presence of catalyst surfaces cracks the polymer into comparatively smaller fractions and at least makes the decomposition of PP energy effective.

4.5. Decomposition kinetics analysis

In the present work, we have carried out nonisothermal decomposition of the PP sample at five different heating rates (5, 10, 15, 20, and 25 K min^{-1}) with the optimum catalyst percentage (18.5 wt%) and without catalyst. The temperature at which the conversion (α) is zero (T_{w0}), decomposition starts (T_d), maximum weight loss rate occurs (T_m) and the end of pyrolysis step ($T_{w\infty}$) takes place have been reported in Table 3 for each case of the experiments. Table 3 reflects that thermal

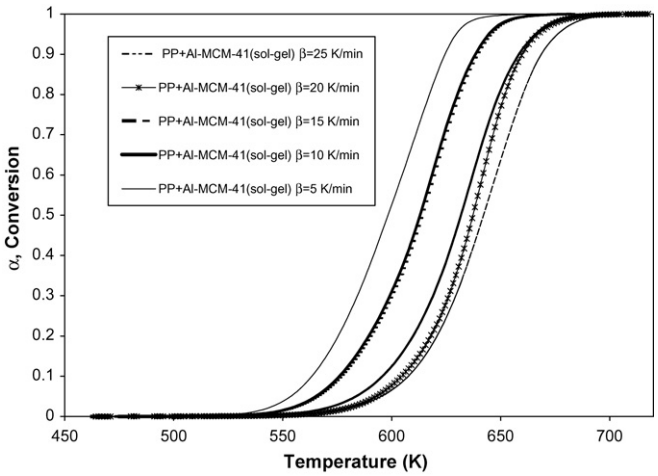

Fig. 11. Variation of conversion (α) with temperature during catalytic nonisothermal pyrolysis (18.5 wt% catalyst) of PP sample.

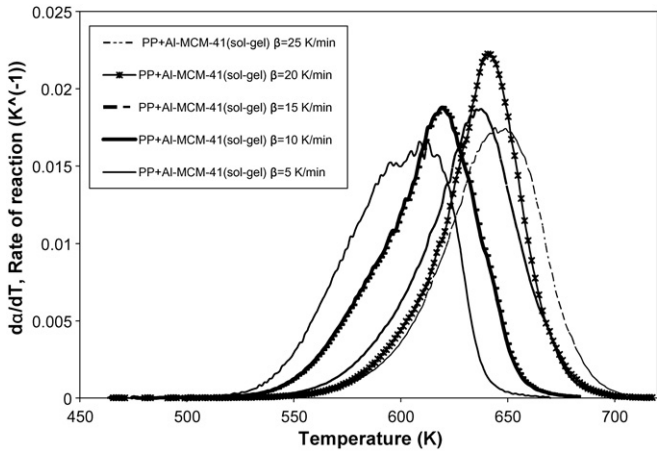

Fig. 12. Variation of rate of decomposition ($d\alpha/dT$) with temperature during catalytic nonisothermal pyrolysis (18.5 wt% catalyst) of PP sample.

decomposition of PP starts at around 670 K and shows a maximum decomposition rate at 723 K at a heating rate of 10 K min^{-1}, which is shifted to much lower temperatures in the presence of catalyst. The shift is observed to be 103 K at a catalyst percentage of 18.5 wt%.

Figs. 9 and 10 represent the TG and DTG curves, respectively for noncatalytic decomposition of PP at five different heating rates of 5, 10, 15, 20, and 25 K min^{-1}. Similarly, Figs. 11 and 12 represent the TG and DTG curves, respectively for catalytic (sol–gel Al-MCM-41) decomposition of PP at five different heating rates of 5, 10, 15, 20, and 25 K min^{-1}. The shift of the TG and DTG (Figs. 9 and 10) curves with heating rate is progressive and approaching towards a limit. We have neglected the minor abnormality observed in the case of catalytic decomposition at 20 K min^{-1} heating rate (Figs. 11 and 12), for simplicity to proceed for the multiple heating rate kinetics analysis which is based on the assumption that the reaction mechanism does not change with heating rate. It is observed from Figs. 10 and 12 that the TG curves mostly show constant pattern behaviour and higher heating rate completes the decomposition faster. The constant pattern behaviour is attributed to the fact of similar reaction mechanism (as discussed earlier), which is the basis of multi-heating rate approach for kinetics analysis [19,21,22,25,26]. This is also supported by the almost similar peak height and constant pattern behaviour of the DTG curves (Figs. 10 and 12) both for the noncatalytic and catalytic decomposition of PP. We can also clearly notice the single peak in the DTG curves both for the catalytic and noncatalytic decomposition of PP. This behaviour is different from our recent studies on ZSM-5 catalyzed decomposition of LDPE [30], where the noncatalytic decomposition showed a single peak at various heating rates but catalytic one showed multiple peaks indicating possible existence of different reaction mechanism. Since single peak is observed at different heating rates for both catalytic and noncatalytic decomposition of PP in the present study, we had approximated it as a single step reaction taking place [17,19]. Accordingly, we found out the single step kinetics triplet or overall kinetics (E, K_0 and n) for both catalytic and noncatalytic decomposition of PP by GA coupled with LOA, fminsearch (HGA) applying different models as mentioned in Table 5 using multi-heating rates.

The traditional optimization techniques and direct and gradient-based search methods to obtain the kinetics parameters through minimization of the square of the deviations between experimental data and calculated values are usually slow and depend strongly on the initial guess. Therefore, frequently the evolution of kinetics parameters is associated with uncertainty due to existence of several false global optima. On the other hand, optimization using HGA is believed to provide the globally optimum parameters which are independent of initial guess values. In fact, in a recent publication on ZSM-5 catalyzed decomposition of waste LDPE [54], we used hybrid genetic algorithm (HGA) and model-free method coupled with local optimization algorithm to get the optimized kinetics triplet. Through that paper we have shown that either of the above approaches works fine for the same. Therefore, in the present paper we have used the (HGA) technique.

All the models listed in Table 5 should be regarded only as semi-empirical formulae and may not fully correspond to real mechanisms of polymer degradation. This is because polymer decomposition is a complicated phenomenon and can be described as occurring by a set of series or parallel chemical reactions via random scission mechanism, chain scission mechanism, etc. According to Mamleev et al. [33], if no information is accessible about the process, a manifold of models should be assumed in order to find the best model(s) both in terms of the minimum deviation between theoretical and experimental data and from the standpoint of physical/chemical sense. Through the present paper we tried to apply, rather than development of any specific model, the available models in the literature to check the most appropriate mathematical description of the PP decomposition behaviour. Thus, for the search of the realistic kinetic parameters and consequently, for a prediction of decomposition behaviour, we inserted into Eq. (1) the empirical functions, $f(\alpha)$ based on the above models to get satisfactory fitting of experimental data. As a consequence we found that the Nucleation and Growth model and the chemical reaction model for specific values of reaction order more closely explains the PP decomposition behaviour under both catalytic and noncatalytic conditions. The initial guesses are taken from the GA. The average kinetics triplet data, based on 15 best sets of data points, for the noncatalytic and

Table 6
Optimum kinetics triplet for PP decomposition with and without of Al-MCM-41 (sol–gel) using HGA

Average values of kinetics parameters	With Al-MCM-41 (sol–gel)	Without Al-MCM-41 (sol–gel)	Model
E (kJ mol^{-1})	128.63	181.48	nth order chemical reaction model
n	0.866	0.901	
K_0	23.737	29.53	
E (kJ mol^{-1})	134.37	187.67	First order chemical reaction model
n	1	1	
K_0	30.698	30.48	
E (kJ mol^{-1})	99.42	146.69	Nucleation and Growth reaction model
n	2/3	2/3	
K_0	18.08	23.64	

Table 7
Activation energy and the effect of different catalysts on PP decomposition temperatures

Sample	Catalysts	E (kJ mol^{-1})	ΔT_m (K)	Reference
PP samples	SM (93.5%)	94	19	[20]
	ST (93.6%)	129	25	
	MO (89.8%)	121	139	Model-fitting method
	SALA (90%)	88	184	
	SAHA (92.5%)	82	184	
	ZSM-12 (30%)	75–105	–	[3] model-free method
	ZSM-5 (50%)	112–130	–	
	Al-MCM-41 (sol–gel) (18.5%)	128.63 (nth order) 128.89 (first order) 99.42 (Nucleation and Growth)	102.8	Present work Model-fitting method

catalytic decompositions are reported through Table 6 for three best-fitted models in terms of AIC_c scores as described. The literature data of activation energies and ΔT_m over different catalysts are reported in Table 7.

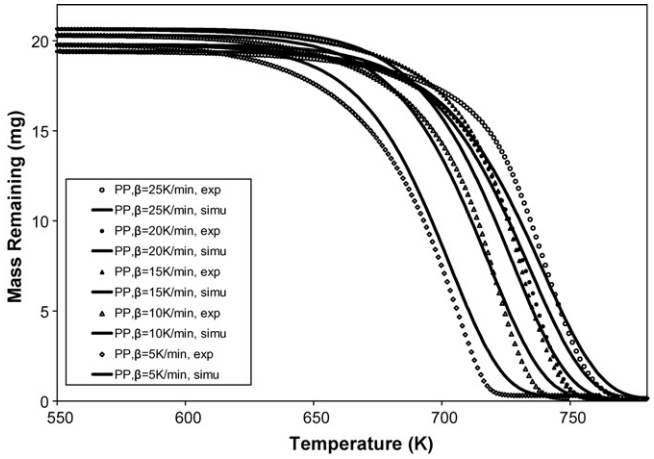

Fig. 13. Comparison between simulated (using HGA predicted kinetics triplet) and experimental mass loss during noncatalytic decomposition of PP at five different heating rates for ***n***th order reaction model (exp, experimental data and simu, simulated data).

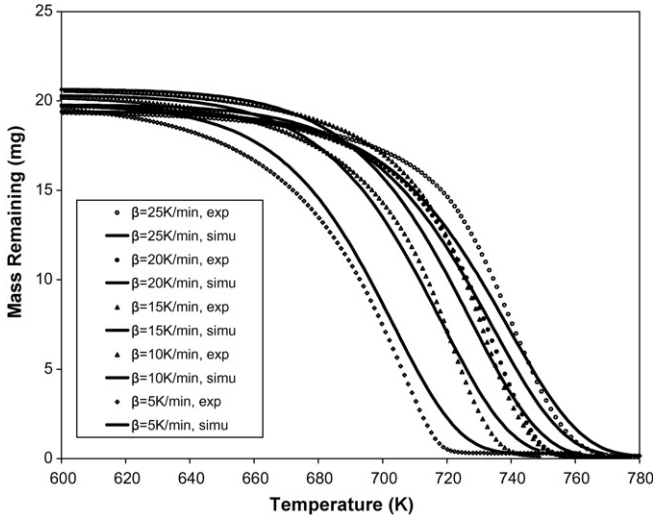

Fig. 14. Comparison between simulated (using HGA predicted kinetics triplet) and experimental mass loss during nonisothermal pyrolysis of PP at five different heating rates for Nucleation and Growth ($n = 2/3$) model (exp, experimental data and simu, simulated data).

4.6. Prediction of experimental TGA data

The kinetics triplets obtained by HGA method employed in the present study are used in simulation to predict the experimental TGA data using different models (Table 5) both for catalytic and noncatalytic decomposition of PP. Corrected Akaike's Information

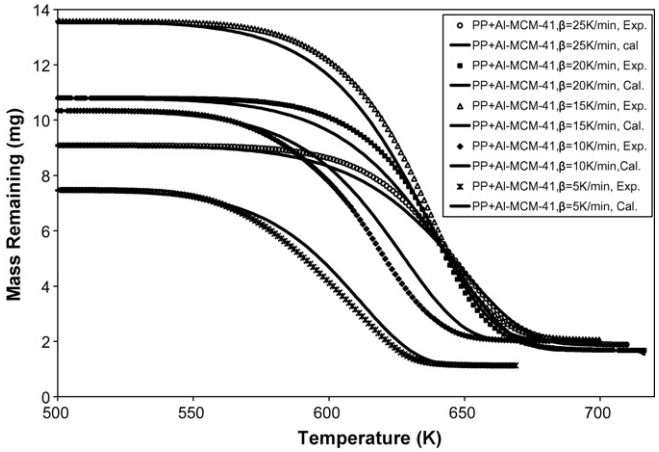

Fig. 15. Comparison between simulated (using HGA predicted kinetics triplet) and experimental mass loss during catalytic decomposition of PP over Al-MCM-41 (sol–gel) catalyst at five different heating rates for ***n***th order reaction model (exp, experimental data and cal, calculated data).

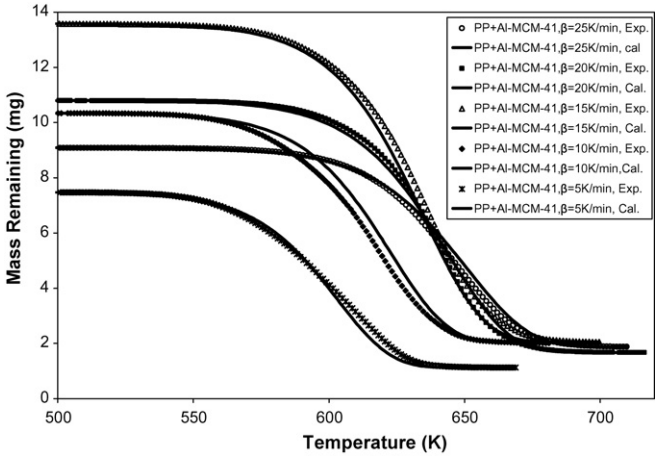

Fig. 16. Comparison between simulated (using HGA predicted kinetics triplet) and experimental mass loss during catalytic decomposition of PP over Al-MCM-41 (sol–gel) catalyst at five different heating rates for Nucleation and Growth model ($n = 2/3$) (exp, experimental data and cal, calculated data).

Criteria [19] is applied to choose the appropriate reaction model. The AIC_c scores are tabulated for all the cases in Table 5. According to the AIC_c scores in Table 5, it is observed that the Nucleation and Growth model with $n = 2/3$ is the best one. Nucleation and Growth model with $n = 1/2$ and the nth order and first order chemical reaction models also show encouraging scores. These observations are also evident from Figs. 13–16, where prediction of the experimental TGA data by the different models is shown for five different heating rates. It is further observed from the figures and AIC_c test that Nucleation and Growth ($n = 2/3$) model is the best one for both catalytic and noncatalytic decomposition of PP and accordingly the obtained kinetics triplets using the model predicted the experimental TGA data most successfully. In fact, the thermal decomposition of PP occurs via initiation, propagation (intermolecular and intramolecular hydrogen transfer and scission) and termination. After the weak links are consumed, the limiting step of the degradation shifts towards the degradation initiated by random scission. Degradation temperature influences the size of the volatile products. As temperature increases, the minimum length of the fragments, which can evaporate under the prevailing conditions, increases. A higher heating rate leads to degradation at higher temperature, which results in a dependence of distribution of size of volatile products on heating rate [24,28]. Thus, the initial stage of polymer decomposition is often accompanied by melting (or softening). At this stage the thermal decomposition can be controlled by the process of formation of a gas phase inside the polymer and by nucleation and nucleus growth in a heterogeneous medium and then diffusion of the formed gas in the subsequent stages [33]. The presence of such mechanism possibly explains the better suitability of the Nucleation and Growth model according to the AIC_c score and also the model prediction of the experimental data. Further, in case of mesoporous Al-MCM-41 catalyzed decomposition, as discussed earlier, the external surface of the catalyst degrades the polymer fragments mentioned above at the start of degradation forming smaller molecules and radicals, which subsequently participate in other reactions like isomerization and oligomerization in the pores of the catalyst. Presence of such mechanism possibly explains the suitability of the reaction model according to the AIC_c score and also the model prediction of the experimental data. However, as opined by Marcilla et al. [34], a good fit of experimental results is not only the criterion to decide upon the decomposition mechanism. Further studies including infrared or mass spectroscopy, a morphology study using SEM or TEM during such decomposition is very much needed to conclude upon the actual reaction mechanism that controls the decomposition behaviour of PP sample.

5. Conclusion

Al-MCM-41 catalysts synthesized by sol–gel and hydrothermal methods are applied for catalytic decomposition of PP. Al-MCM-41 (sol–gel) catalysts showed better performance in terms of reduction of maximum decomposition temperature possibly due to more surface area. Reusability studies with 17.0 wt% Al-MCM-41 (sol–gel) catalysts indicate marginal loss of activity of the catalyst even after reusing seven times. Detailed investigation with different Al-MCM-41 (sol–gel) catalyst percentage reveals 18.5 wt% Al as the optimum catalyst percentage for decomposition of PP, after which the change in maximum decomposition temperature is not so significant.

Further decomposition studies of PP under both noncatalytic and catalytic conditions (18.5 wt% Al-MCM-41 (sol–gel) catalysts) are conducted at five different heating rates to evaluate the kinetics parameters. The constant pattern behaviour of the TG curves for different catalyst percentages and different heating rates possibly suggests existence of similar reaction mechanism both under catalytic and noncatalytic decomposition of mesoporous Al-MCM-41. Here, large polymer fragments are cracked on the external surface of the catalyst and then enter into the mesopores where they get cracked further leading mainly to the higher olefins and liquid products. This can only be confirmed after thorough analysis of the decomposition products. However, the presence of catalyst surfaces cracks the polymer into comparatively smaller fractions and at least makes the decomposition of PP energy effective.

The hybrid genetic algorithm (HGA) was used to estimate the globally optimum overall kinetics parameters using 15 different decomposition models reported in the literatures. The suitability of the models is tested using the AIC_c score. Results show that the Nucleation and Growth model with reaction order, $n = 2/3$ better predicted the experimental TGA data. However, the Nucleation and Growth model with $n = 1/2$ and nth order model also show good AIC_c score and predicted well the experimental TGA data. Thus, though apparently it seems that the Nucleation and Growth model controls the decomposition of PP sample, further detailed investigation including infrared or mass spectroscopy, and a morphology study using SEM or TEM during such decomposition is essential to conclude upon the actual reaction mechanism that controls decomposition of the PP sample.

References

[1] G. Karishma, M. George, Polym. Degrad. Stab. 86 (2004) 225–231.
[2] A. Marcilla, A. Gómez, J.A. Reyes-Labarta, A. Giner, F. Hernández, J. Anal. Appl. Pyrol. 68/69 (2003) 467–480.
[3] J.G.A.P. Filho, E.C. Graciliano, A.O.S. Silva, M.J.B. Souza, A.S. Araujo, Catal. Today 107/108 (2005) 507–512.
[4] Q. Zhou, L. Zheng, Y.Z. Wang, G.M. Zhao, B. Wang, Polym. Degrad. Stab. 84 (2004) 493–497.
[5] A. Durmus, S.N. Koc, G.S. Pozan, A. Kasgoz, Appl. Catal. B 61 (2005) 316–322.
[6] C. Vasile, H. Pakdel, B. Mihai, P. Onu, H. Darie, S. Ciocâlteu, J. Anal. Appl. Pyrol. 57 (2001) 287–303.
[7] A. Marcilla, A. Gómez-Siurana, D. Berenguer, Appl. Catal. A 301 (2006) 222–229.
[8] Y.H. Lin, H.Y. Yen, Polym. Degrad. Stab. 89 (2005) 101–108.
[9] P. Onu, C. Vasile, S. Ciocilter, E. Iojoiu, H. Darie, J. Anal. Appl. Pyrol. 49 (1999) 145–153.
[10] Y.H. Lin, M.H. Yang, Appl. Catal. B 69 (2006) 145–153.
[11] J. Aguado, D.P. Serrano, J.M. Escola, E. Garagorri, J.A. Fernández, Polym. Degrad. Stab. 69 (2000) 11–16.
[12] A. Marcilla, A. Gómez, J.A. Reyes-Labarta, A. Giner, F. Hernández, Polym. Degrad. Stab. 80 (2003) 233–240.
[13] R.A. García, D.P. Serrano, D. Otero, J. Anal. Appl. Pyrol. 74 (2005) 379–386.
[14] J. Aguado, D.P. Serrano, G. San Miguel, J.M. Escola, J.M. Rodríguez, J. Anal. Appl. Pyrol. 78 (2007) 153–161.
[15] D.P. Serrano, J. Aguado, J.M. Escola, J.M. Rodríguez, G. San Miguel, J. Anal. Appl. Pyrol. 74 (2005) 370–378.
[16] R.V. Grieken, J.M. Escola, J. Moreno, R. Rodríguez, Appl. Catal. A: Gen. 305 (2006) 176–188.
[17] B. Saha, A.K. Ghoshal, Chem. Eng. J. 111 (2005) 39–43.
[18] B. Saha, A.K. Maiti, A.K. Ghoshal, Thermochim. Acta 444 (2006) 46–52.
[19] B. Saha, A.K. Ghoshal, Ind. Eng. Chem. Res. 45 (2006) 7752–7759.
[20] P. Carniti, A. Gervasini, Thermochim. Acta 379 (2001) 51–58.
[21] S. Vyazovkin, V. Goriyachko, Thermochim. Acta 194 (1992) 221–230.
[22] S. Vyazovkin, C.A. Wight, Thermochim. Acta 340/341 (1999) 53–68.
[23] S. Vyazovkin, Thermochim. Acta 355 (2000) 155–163.
[24] S. Vyazovkin, C.A. Wight, Chem. Mater. 11 (1999) 3386–3389.
[25] S. Vyazovkin, D. Dollimore, J. Chem. Inf. Comput. Sci. 36 (1996) 42–45.
[26] S. Vyazovkin, Int. J. Chem. Kinet. 28 (1996) 95–101.
[27] S. Vyazovkin, N. Sbirrazzuoli, Macromol. Rapid Commun. 27 (2006) 1515–1532.
[28] J.D. Peterson, S. Vyazovkin, C.A. Wight, Macromol. Chem. Phys. 202 (2001) 775–784.
[29] B. Saha, A.K. Ghoshal, Thermochim. Acta 451 (2006) 27–33.
[30] B. Saha, A.K. Ghoshal, Thermochim. Acta 453 (2007) 120–127.
[31] V. Mamleev, S. Bourbigot, Chem. Eng. Sci. 60 (2005) 747–766.
[32] J. Lefebvrea, V. Mamleev, M.L. Brasa, S. Bourbigot, Polym. Degrad. Stab. 88 (2005) 85–91.

[33] V. Mamleev, S. Bourbigot, M. Le Bras, S. Duquesne, J. Šesták, Phys. Chem. Chem. Phys. 2 (2000) 4708–4716.
[34] A. Marcilla, J.C. García-Quesada, R. Ruiz-Femenia, Thermochim. Acta 445 (2006) 92–96.
[35] M.E. Brown, M. Maciejewski, S. Vyazovkin, R. Nomen, J. Sempere, A. Burnham, J. Opfermann, R. Strey, H.L. Anderson, A. Kemmler, R. Keuleers, J. Janssens, H.O. Desseyn, C.R. Li, T.B. Tang, B. Roduit, J. Malek, T. Mitsuhashi, Thermochim. Acta 355 (2000) 125–143.
[36] H.J. Flammersheim, J.R. Opfermann, Thermochim. Acta 337 (1999) 141–148.
[37] J.R. Opfermann, E. Kaisersberger, H.J. Flammersheim, Thermochim. Acta 391 (2002) 119–127.
[38] A.K. Burnham, J. Therm. Anal. Cal. 60 (2000) 895–908.
[39] R. Capart, L. Khezami, A.K. Burnham, Thermochim. Acta 417 (2004) 79–89.
[40] S. Katare, A. Bhan, J.M. Caruthers, W.N. Delgass, V. Venkatasubramanian, Comput. Chem. Eng. 28 (2004) 2569–2581.
[41] L. Balland, L. Estel, J.M. Cosmao, N. Mouhab, Chemometr. Intell. Lab. Syst. 50 (2000) 121–135.
[42] G. Rein, C. Lautenberger, A.C. Fernandez-Pello, J.L. Torero, D.L. Urban, Combust. Flame 146 (2006) 95–108.
[43] S.D. Harris, L. Elliott, D.B. Ingham, M. Pourkashanian, C.W. Wilson, Comput. Methods Appl. Mech. Eng. 190 (2000) 1065–1090.
[44] L. Elliotta, D.B. Inghama, A.G. Kyneb, N.S. Merab, M. Pourkashanianc, C.W. Wilson, Prog. Energy Combust. Sci. 30 (2004) 297–328.
[45] L. Elliott, D.B. Ingham, A.G. Kyne, N.S. Merab, M. Pourkashanian, S. Whittake, Comput. Chem. Eng. 30 (2006) 889–900.
[46] T.Y. Park, G.F. Froment, Comput. Chem. Eng. 22 (Suppl.) (1998) S103–S110.
[47] D.B. Hibbert, Chemometr. Intell. Lab. Syst. 19 (1993) 319–329.
[48] P.K. Gudla, R. Ganguli, Appl. Math. Comput. 167 (2005) 1457–1474.
[49] MATLAB help, version 7.0.0.19920 (R14), The MathWorks, Inc., Natick, MA, 2004.
[50] A. Matsumoto, H. Chen, K. Tsutsumi, M. Grün, K. Unger, Micropor. Mesopor. Mater. 32 (1999) 55–62.
[51] M.M.L. Ribeiro Carrott, F.L. Conceição, J.M. Lopes, P.J.M. Carrott, C. Bernardes, J. Rocha, F. Ramôa Ribeiro, Micropor. Mesopor. Mater. 92 (2006) 270–285.
[52] R.H.P.R. Poladi, C.C. Landry, J. Solid State Chem. 167 (2002) 363–369.
[53] J. Aguado, D.P. Serrano, J.M. Escola, Micropor. Mesopor. Mater. 34 (2000) 43–54.
[54] B. Saha, A.K. Ghoshal, Ind. Eng. Chem. Res. 46 (2007) 5485–5492.